



Paleoenvironments and origin of the sedimentary phosphorites of the Napo Formation (Late Cretaceous, Oriente Basin, Ecuador)

M.E. Brookfield^{a,*}, D.P. Hemmings^b, P. Van Straaten^c

^a *Institute of Earth Sciences, Academia Sinica, P.O. Box 1-55, Taipei 11529, Taiwan, ROC*

^b *Jacques Whitford Limited, 7271 Warden Avenue, Markham, ON, Canada L3R 5X5*

^c *Land Resource Science, Guelph University, Guelph, ON, Canada N1G 2W1*

ARTICLE INFO

Article history:

Received 29 April 2008

Accepted 11 February 2009

Keywords:

Paleoenvironments

Origin

Napo

Phosphorites

Late Cretaceous

Ecuador

ABSTRACT

The Napo phosphorites were deposited at the edge of a stable marine shelf during the Upper Cretaceous (Coniacian) oceanic anoxic event (OAE 3) at the transition from bioclastic limestone to organic-rich shale facies. Phosphogenesis was triggered in the shelf margin environment by a number of factors including strong upwelling currents, high biological activity, plankton blooms, and large amounts of organic matter production and subsequent accumulation. Dissolved phosphate levels increased in the sediment from a combination of anoxic conditions and microbial activity. Once dissolved phosphate concentrations were high enough, apatite began to form around nucleic sites including mineral grains, shells, wood fragments, and foraminifera tests forming peloidal fluorine rich carbonate fluoroapatite (francolite). As the peloids formed, sedimentation continued and dissolved phosphate concentrations diminished. A period of minor winnowing ensued, and as dissolved phosphate concentrations remained low, shale layers were deposited separating the various phosphate layers.

© 2009 Elsevier Ltd. All rights reserved.

1. Introduction

In the late 1970s, Ecuador had nearly depleted all of its guano phosphate deposits, and exploration for phosphate reserves was started in the eastern part of the country in the Oriente Basin. While a number of phosphorites were identified, none have been mined to date: as a result, Ecuador relies on imported phosphate fertilizers from Colombia, Peru and other countries. The Cretaceous (late Albian to ? Campanian) Napo Formation consists of a succession of marine mudstones, limestones and sandstones whose upper part contains phosphate layers between limestone and mudstone (Wilkinson, 1980; Vera, 2001). The A-series phosphate layers in this upper part contain three distinct phosphate layers with between 22% and 24% phosphate and could potentially supply local farmers with indigenous phosphate fertilizers. This paper concentrates on the description and paleoenvironments of the Napo Formation and its phosphate deposits, and its relevance for models of shelf phosphate genesis.

2. Materials and methods

Fresh phosphorite samples were obtained from an abandoned mine drift, 80 km west of Lago Agrio, Ecuador. Twenty thin sections

(30 microns thick) were made from representative layers within the Upper Napo Formation, and thirteen thin sections were made from the base, middle and upper parts of each phosphate layer and interbedded shales in the mine gallery.

Microprobe analysis of thin sections was performed in the microscopy laboratory in the Earth Science Department at the University of Western Ontario with the assistance of Dr. Menghua Liu. Thin sections were coated with a thin layer (150 µm) of carbon by the Edwards Auto 306 coater, and were studied under the JEOL JXA8600 Superprobe. The microprobe provides quantitative analysis by bombarding a focused electron beam (5 nm in diameter) on the thin section under an accelerating voltage of 15 kV. The emitted X-rays are detected using a germanium detector. The X-ray data obtained from the Napo phosphorites were compared with those obtained from the Durango apatite (Mexico) standard. Analysis performed by using the Energy Dispersion Spectrometer (EDS) Quantum MGA 4000, provided immediate qualitative elemental data at specific locations on the thin section determining the composition of the selected minerals.

Two separate sets of X-ray fluorescence data on Napo phosphorite and interbedded layers were obtained. The first data set was taken from a report on the Napo Phosphates (Ministerio de Recursos Naturales y Energeticos Direccion General de Geologia y Minas, 1985). The second set was generated from XRF analyses of different samples performed at the University of Western Ontario. Samples were ground to a talc-like consistency using a motorized agate mortar and pestle and pressed into a slide, which were then placed

* Corresponding author.

E-mail addresses: mbrookfi@hotmail.com (M.E. Brookfield), DHemming@jacqueswhitford.com (D.P. Hemmings), pvanstra@uoguelph.ca (P. Van Straaten).

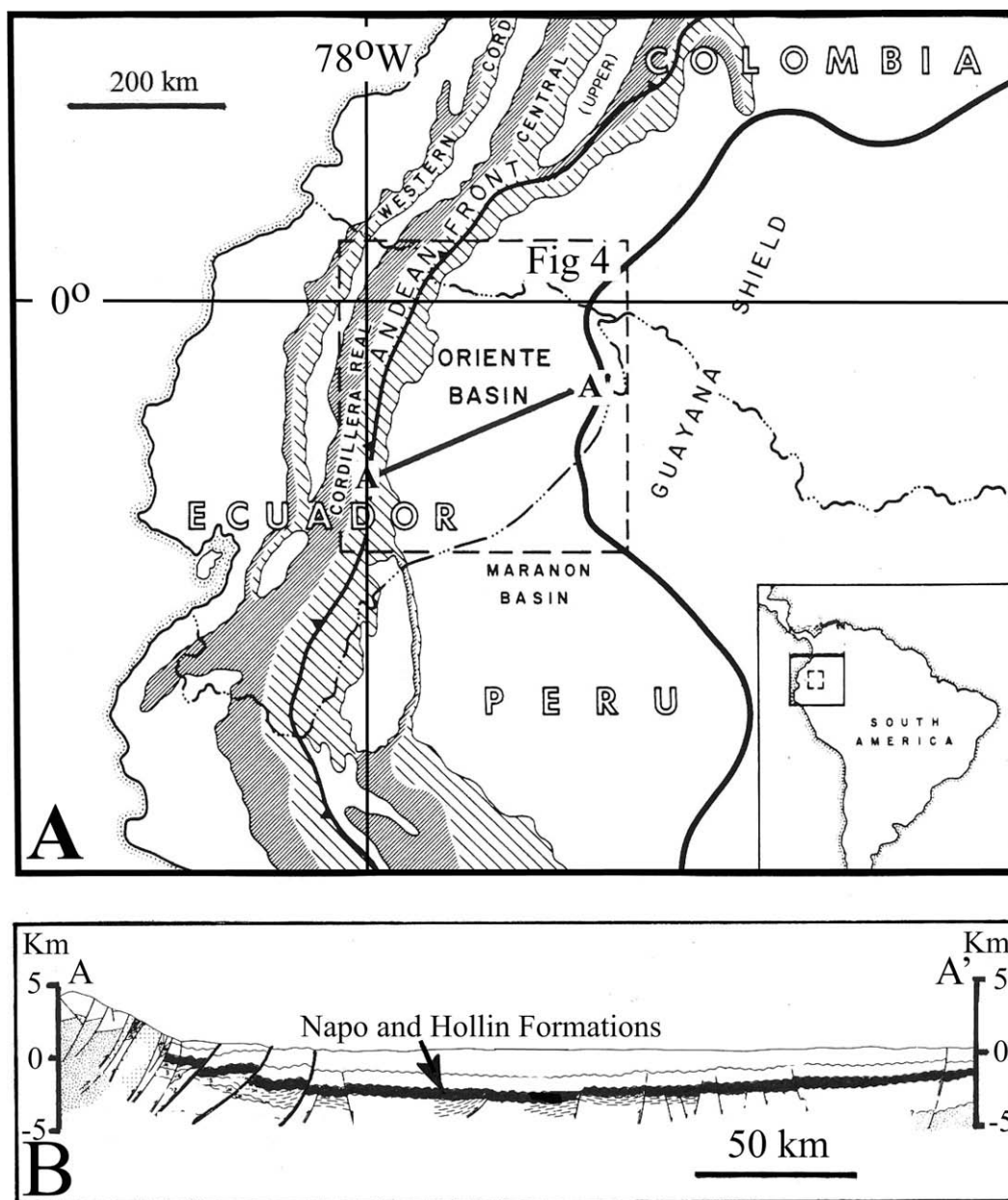


Fig. 1. (A) Location map of the Oriente Basin with reference to structural units. (B) Structural cross-section of the Oriente Basin.

in the XRF machine for analyses. The X-rays emitted by the samples were measured and compared with the intensity of X-rays from standards.

Neutron activation analysis (NAA) was performed at Actlab, Ancaster, Ontario, on selected samples taken from two vertical transects (7 and 16), and from two radioactive hot spots in samples from the middle A2 phosphate layer (see below p. 10–11). Samples were prepared by first crushing them to a talc-like consistency with a rock pulveriser and motorized ball crusher. NAA was then performed on the samples and analyzed for uranium, thorium, zinc, chromium, barium, and rare-earth elements of lanthanum, cerium, and neodymium.

Inductively coupled plasma optical emission spectroscopy (ICP-OES) was performed on the selected samples from the two vertical transects to determine total phosphorus, potassium, and sulfur concentrations. Samples were first ground to a talc-like consistency using a rock pulveriser and motorized ball crusher. Aqua-re-

gia digests were then performed on the samples, and were subsequently analyzed with ICP-OES at the University of Western Ontario. The Napo phosphate rock samples were prepared for crystallographic unit cell *a*-dimensions (*a*-values) determination according to procedures based on McClellan and Lehr, 1969. The *a*-values reflect the degree of carbonate substitution within the apatite crystal structure. Rock samples were first prepared by loosely crushing and sorting according to grain size using a rock pulveriser, motorized agate mortar and pestle and 0.01 to 2 mm sieves. A modified version of the Silverman solution was then used on the sorted grains by applying dilute (5% HCl) acid to remove the carbonates from the francolite peloids. Individual francolite peloids were then identified and separated under a Nikon SMZ-10 microscope using a needle and Schott KL-1500 portable light source. Once separated, francolite grains were crushed to a talc-like consistency using a motorized ball crusher. The samples were then analyzed using X-ray diffraction with a Cobalt Rigaku Gigerflex

operating at 40 Kv and 25 milliamps. D-spacings were then determined using JADE software and were imported into UnitCell, an a-cell parameter software to determine the a-value.

Mineralogy and geochemistry were done with microprobe analysis, X-ray fluorescence (XRF), neutron activation analysis (NAA). Inductively coupled plasma optical emission spectroscopy (ICP-OES) was performed on the selected samples to determine total phosphorus, potassium, and sulfur.

Further selected samples were prepared as mentioned above and were then analyzed for organic carbon content with a Leco Furnace at Analytical Laboratory Services, University of Guelph. From the total carbon content inorganic and organic carbon levels were determined and recorded.

3. Geological background

The Oriente Basin covers about 100,000 km² and now lies across the shield, sub-Andean and Andean zones of Colombia, Ecuador and Peru (Fig. 1A) (Dashwood and Abbots, 1990). It is underlain by thinned Precambrian rocks of the Guyana shield and presently has two distinct geological and geomorphological zones, a sub-Andean zone to the west adjacent to the Andes, and an Upper Amazon zone to the east, which were formed during Andean tectonic deformation during the late Cenozoic (Baldock,

1985). The Oriente Basin has the most important oil reservoir found in Ecuador, in the Cretaceous Napo Formation (Feininger, 1975), which also hosts the economic phosphate deposits studied in this paper.

As South America split from Africa in mid-Jurassic times and started moving westwards, magmatic arcs developed on and off the western South America margin. Extension behind these eventually produced the original back-arc Oriente Basin. Rifting began in the mid-Jurassic and was followed by the establishment of a marginal basin spreading ridge in the earliest Cretaceous whose extension continued into the latest Cretaceous (Lebrat et al., 1986). Deformation and uplift in the Andes to the west, beginning in the early Cenozoic led to the deposition of thick, unconformity bounded synorogenic coarse clastic successions, and progressive deformation of both Mesozoic and Cenozoic sediments across the basin (Feininger and Bristow, 1980) (Fig. 1B).

During the Jurassic and Cretaceous, the entire Amazon Basin was located on a submerged continental shelf underlain by cratonic rocks of the Guyana Shield (Feininger, 1975; Kennerley, 1980; Clapperton, 1993). In the sub-Andean zone, sedimentation began in the early Jurassic with the deposition of the largely carbonate Santiago Formation (Kennerley, 1980). Following mid-Jurassic uplift, and rifting, regional crustal collapse and extension formed rift valleys in which up to 500 m of coarse continental

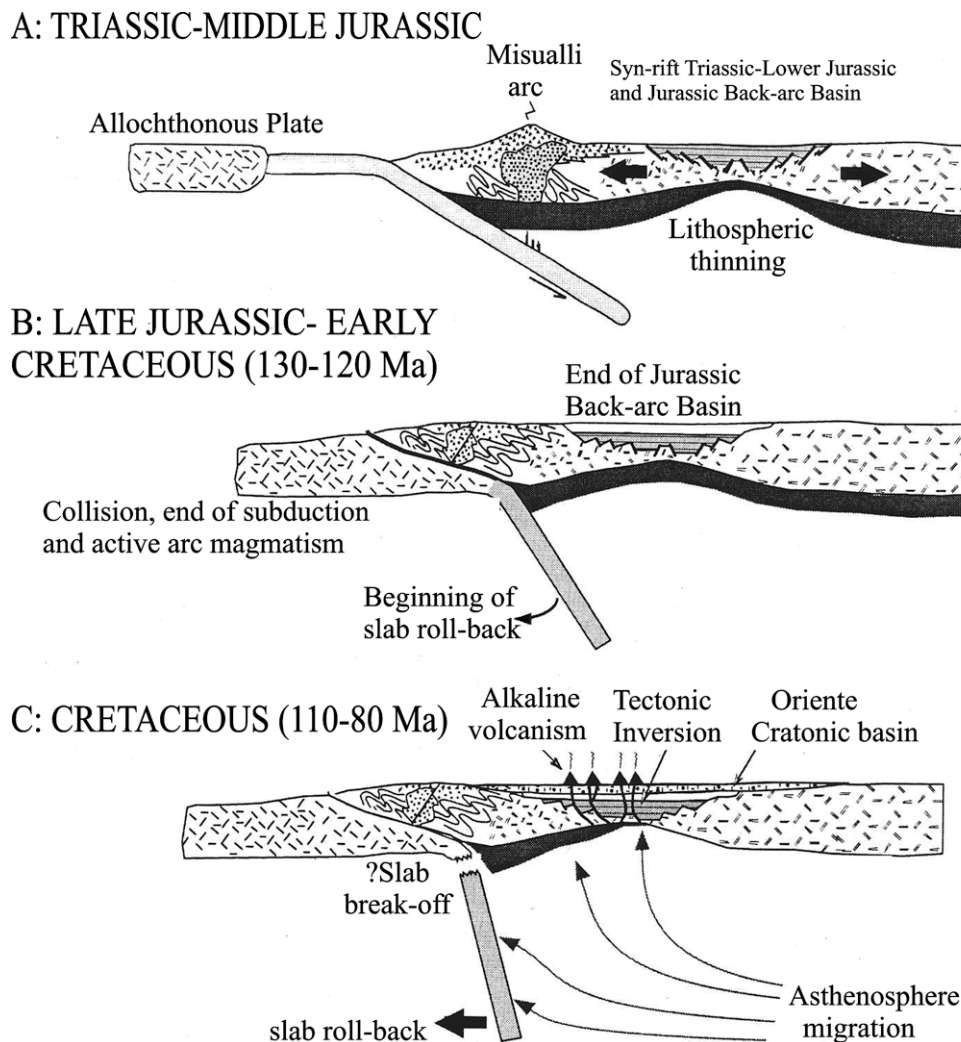


Fig. 2. Restored cross-section showing Mesozoic evolution of Ecuador (after Kennerley, 1980).

ERA	PERIOD	EPOCH	FORMATION	MEMBER		DOMINANT LITHOLOGY		
MESOZOIC	CRETACEOUS	CENOMANIAN-CAMPANIAN	NAPO	TENA			RED BEDS	
						BASAL TENA SD		
				UPPER NAPO	M-1 SAND		QTZ. SS.	
				MIDDLE NAPO	NAPO SHALE		DK. GRAY SHALES	
					Phosphate horizon M-2 SAND		MICRITIC LMST. QTZ. GLAUC. SS.	
				LOWER NAPO	"A" LMST		MICRITIC LMST.	
					UPPER "U"		QTZ SS. & DK. GRAY SHALE	
				BASAL NAPO	LOWER "U"		DK. GRAY SHALE & LMST.	
					"T" SAND		QTZ. GLAUC. SS.	
					BASAL NAPO		DK. GRY SHALE, GLAUC. SS, LMST. STRINGERS	
				APT./ALB	HOLLIN			QTZ. SS.
				PRE - HOLLIN				

Fig. 3. Cretaceous stratigraphy and terminology of the Central Oriente Basin, Ecuador (from Hunter et al. (2000)).

clastics of the Chapiza Formation accumulated capped by pyroclastic sediments (Dashwood and Abbots, 1990). In the lowermost Cretaceous, marine transgression inaugurated the deposition of Aptian to Coniacian mixed shelf, slope and basinal clastic-carbonate units in the retro-arc basin and on the continental shelf (Fig. 2) (Baldock, 1985). Sedimentation was primarily controlled by marine transgressions and regressions on the shelf (Tschopp, 1956). The Hollin Formation (Aptian–Albian) rests with angular unconformity on the Chapiza Formation, while the overlying Napo Formation (Albian–Coniacian) is unconformably overlain by the red-beds of the Maestrichtian to ? Palaeocene Tena Formation, which marks the start of major deformation in the Andean range (Fig. 3). Later Tertiary deposition occurred in a number of fault-bounded basins extending the length of South America from Peru to Panama (Feininger and Bristow, 1980).

The Hollin Formation (Aptian–Albian) consists of homogeneous thick-bedded quartz sandstones, with only minor, but laterally persistent, carbonaceous mudstone and coal interbeds (Dashwood and Abbots, 1990). In the southwestern part of the basin it is 150 m thick, and it thins northeastward onto the Guyana Shield where it becomes indistinguishable from the overlying basal Napo Formation sandstones. The Hollin Formation was deposited as the result of early Cretaceous marine transgression from the western marginal sea over the block-faulted and peneplaned Guyana Shield, which was followed by stillstand and/or regressive conditions in which fluvial, braided and littoral mature sandstone with their interbedded mudstones and coals were deposited (Dashwood and Abbots, 1990; Kummert and Casal, 1986).

The Napo Formation (late Albian– early Campanian, around 105–83 Ma) (Vallejo et al., 2002) is one of the main hydrocarbon-

bearing units in the Oriente Basin, and contains some of the most prolific hydrocarbon source rocks in South America (White et al., 1995). The consequently good surface and subsurface studies form an excellent framework for evaluating its phosphate beds (Fig. 4). The Napo Formation varies in thickness from 200 to over 700 m and was originally divided into three distinct units by Tschopp (1953). More detailed studies during extensive oil exploration led to a fourfold subdivision into Basal, Lower, Middle, and Upper Napo Formation (Jaillard, 1996).

In general, thick successions of dark grey limestones, black shales, and glauconitic sandstones together with phosphorites occur in the west and pass eastwards into thinner sandstone-dominated deltaic and fluvial successions (Feininger, 1975; Wilkinson, 1980; Hunter et al., 2000) (Fig. 4).

The Basal Napo Formation (Late Albian) consists of a sandstone-dominated succession of alternating sandstones, shales, limestones, and cherts up to 175 m thick (Jaillard, 1996). The lower sandstones are glauconitic, fine to medium grained, and in places contain laminated shales or mudstones. They are transitional to, and indistinguishable from, the Hollin Formation in the east (Sanders, 2001).

The Lower Napo (latest Albian–Cenomanian) consists of a mixed sandstone, shale and limestone succession up to 150 m thick.

The Middle Napo (mid-Turonian – ? earliest Coniacian) is dominated by bioclastic limestones and shales with subordinate sandstones, is up to 100 m thick, and has erosional contacts with the units above and below the Lower Napo (Jaillard, 1996). The Middle Napo M2 Limestone on which the Upper Napo phosphorite was deposited shows dominantly marine particulate organic matter

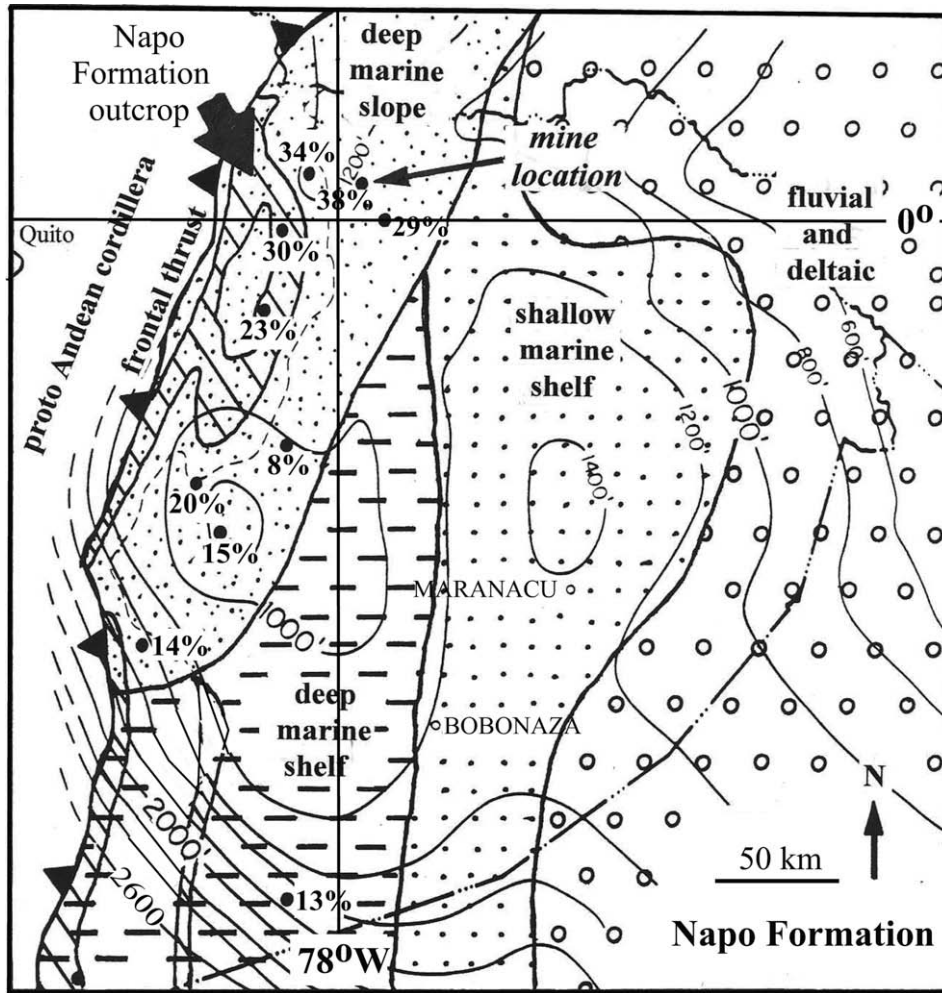


Fig. 4. Isopachs (in feet), outcrops, and overall facies distributions for the entire Napo Formation. Dots show Napo phosphate exposures with maximum phosphate content in per cent; and location of mine studied (based on Dashwood and Abbots (1990) and Wilkinson (1980)).

(POM) and contains the Santonian calcareous nannofossil, *Lithastrinus septenarius* (Vallejo et al., 2002). However, it also contains an

early Coniacian macrofauna which may be more reliable as to age (Jaillard et al., 2005).

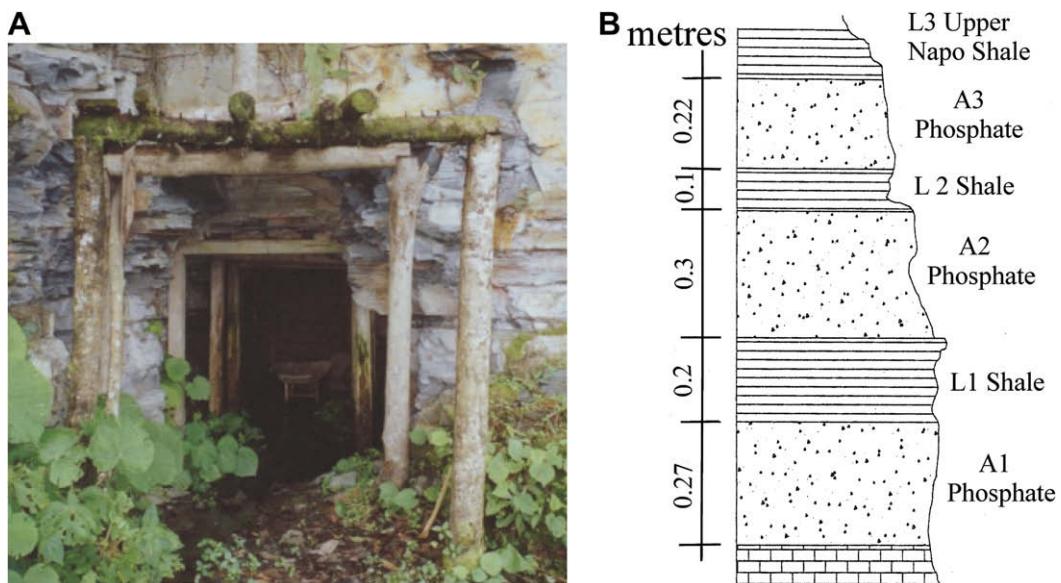


Fig. 5. (A) View of mine gallery; (B) stratigraphic column of Napo Formation phosphate horizon at mine gallery.

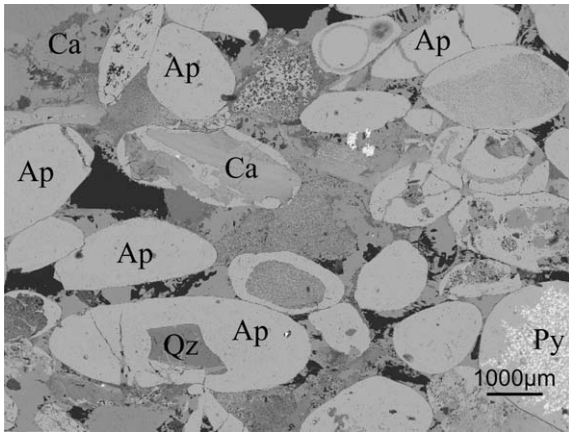


Fig. 6. Thin section of A2 phosphate layer: Ap, apatite, Ca, calcite, Qz, quartz; Py, pyrite; scale bar is 1000 μm.

The Upper Napo (late Coniacian–Santonian) is dominated by shale with subordinate limestone and sandstone, and is up to 250 m thick (Vera, 2001; Jaillard et al., 2005).

There are two orders of transgressive/regressive cycles in the Basal to Middle Napo. Large-scale transgressive limestone/shale packages of the Basal Napo, B limestone, A limestone, and M2 limestone, alternate with the regressive T sandstones, U sandstones, and M2 sandstones packages (sequences) (Fig. 3). The transgressive packages consist of marine bioclastic limestones and shales that pass laterally into sandstones which extend to the eastern limits of the area during maximum transgression. The regressive package consists of fluvial sandstone which grade westwards into deltaic clastics and is bounded by regional erosional sequence

boundaries (Hunter et al., 2000). The fluvial sandstone interpretation is based on the dominance of fine- to medium grained planar cross-bedded (dips 10–20°) granular sandstones containing basal mudstone clasts but with a lack of interbedded fine grained units (Shanmugam et al., 2000). Such characteristics suggest deposition by low-sinuosity streams. These grade up, through transitional units into fine- to medium grained sometimes herringbone cross-bedded sandstones with abundant mud drapes and crinkled laminae. The sandstones bodies show east–west orientations. Such characteristics, especially the reversing currents shown by the cross-beds, indicates tidal sand bodies (Saito, 2001; Shanmugam et al., 2000). The upward transition from fluvial channels to tidal bodies within widespread sedimentary units indicates deposition in a tidally controlled delta, where tides transport sand via funnel-shaped distributaries onto adjacent shelves and a transgressive trend (Kulp et al., 2007). Further west, marine sandstones and shales have gradational relationships with underlying limestones. These sandstones contain glauconite which forms on present-day delta front shelves and slopes in cool waters from 50 to 500 m in depth (Odin, 1985) and sometimes in upwelling environments (Wigley and Compton, 2006). Smaller-scale transgressive and regressive sequences (parasequences) occur within the larger sequences. A paleogeographic sketch showing facies relationships for the Basal Napo (Fig. 4) applies reasonably well to the Basal to Middle Napo units.

The Upper Napo, which contains the phosphate deposits, is predominantly a marine limestone–shale succession dominated by marine particulate organic matter (POM), though with increased terrestrial POM compared to the units mentioned below (Vallejo et al., 2002). The top M1 sand has the same characteristics as the lower Napo sands (Shanmugam et al., 2000). The Upper Napo is inferred to have accumulated in a deeper but still land-influenced

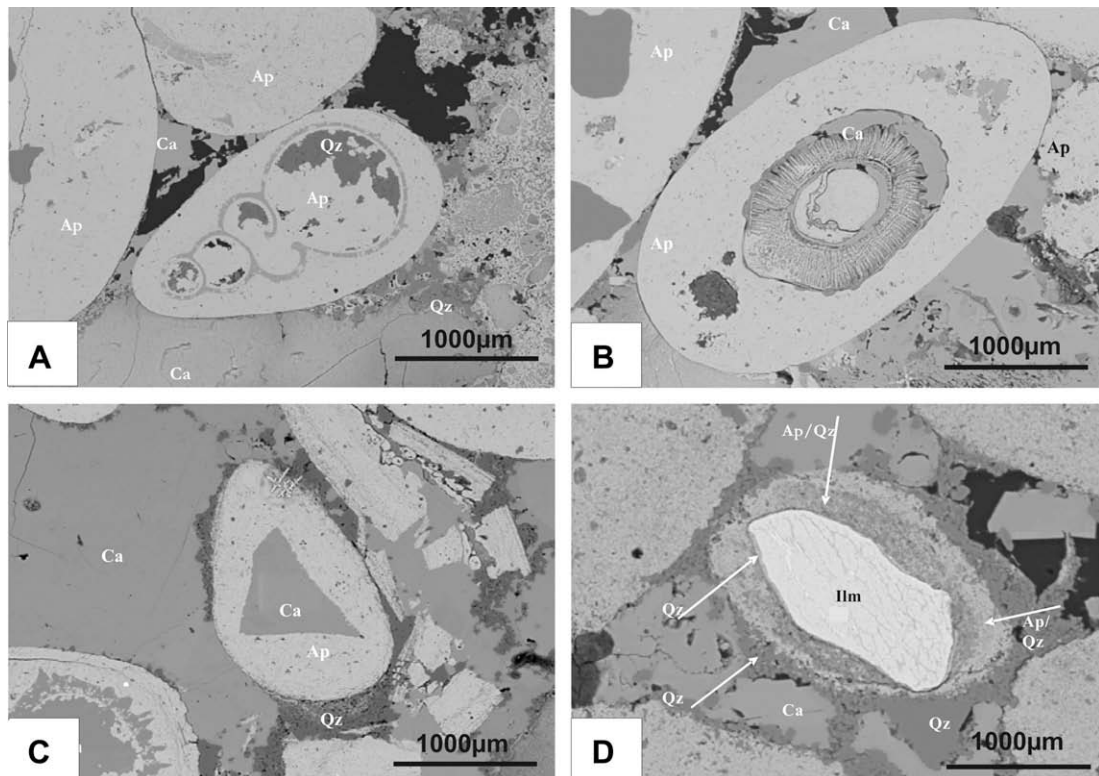


Fig. 7. Phosphate peloid nuclei: (A) aragonitic pteropod with silica replacement, (B) plant fragment, (C) angular calcite and (D) Ilmenite with silica replacement of peloid; scale bar is 1000 μm.

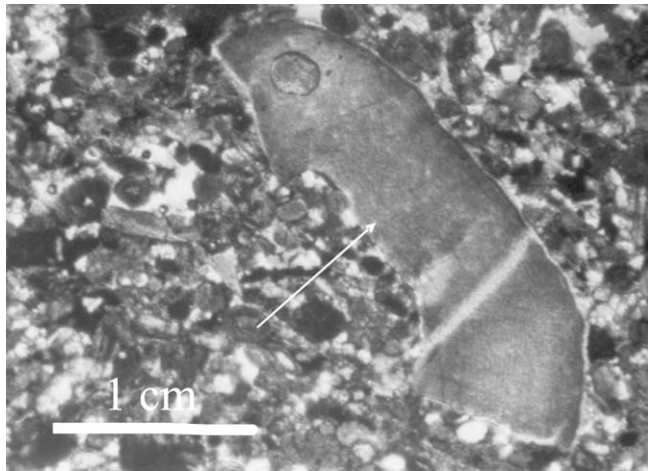


Fig. 8. Phosphatized wood fragment, two centimeters long, in sandy phosphatic matrix.

marine shallowing upwards environments. Its base marks the maximum transgression (or flooding event) in the Napo Formation (Jaillard et al., 2005) and it is here that the phosphorite deposits occur.

4. Napo phosphorites

The Napo phosphorites occur as thin units near the base of the Upper Napo unit (Feininger, 1975). The most extensive phosphorites occur in a belt on the westward side of the shale sea before sediments thicken into the retro-arc basin trough (Fig. 4). They occur as thin interbeds within black shales above the limestone horizons. In order to get fresh specimens, we studied the Napo phosphorites in detail at an exploratory mine gallery 80 km west of Lago Agrio (Fig. 4). The gallery is 8.2 m long, 1.6 m high and 1.5 m high and lies a few hundred meters off a gravel road on a donkey trail (Fig. 5).

The phosphate layers (A1, A2, and A3) are coarse to fine grained, moderately sorted to well sorted, dark grey to brown peloidal rocks: fresh rocks are compact and hard, whereas weathered rocks are soft and brittle. The phosphate layers lie interbedded with black shales between the limestone and overlying black shales, but in fact the phosphate and shale lithologies grade into one another. The A1 phosphate layer consists of moderately sorted, medium to coarse-grained peloids, and contains minor shale laminations at its base and top. It coarsens upwards from small tightly packed peloids with abundant wood and shell fragments but little organic matter, to larger more loosely packed peloids up to 1.5 mm in diameter with organic laminae in-between. The L1 planar-laminated black shale layer contains scattered phosphate peloids, moderately rounded and sub-rounded calcite

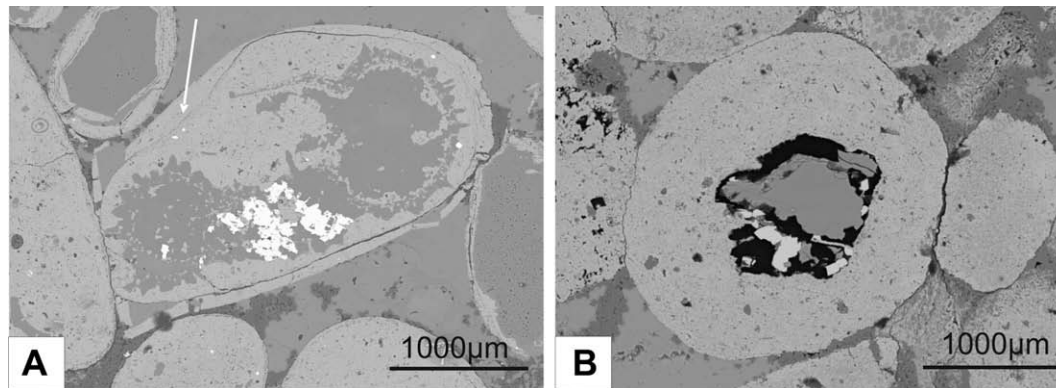


Fig. 9. Diagenetic changes: (A) silica replacement and coatings (arrowed) on apatite peloids, (B) second generation francolite growth in partially silica replaced peloid. Scale bar is 1000 μm .

Table 1
Major element oxides from layers of the phosphorite horizon (XRF).

Sample (Wt%)	LOI	SiO ₂	P ₂ O ₅	Fe ₂ O ₃	Al ₂ O ₃	K ₂ O	Na ₂ O	CaO	MgO	MnO	Total	Organic matter
Shale L1	19.9	44.72	.94	1.31	4.49	.16	.16	25.54	.93	.02	98.25	4.28
Shale L2	14.9	52.64	7.72	1.24	2.74	.18	.18	17.44	1.04	.02	98.11	8.47
Shale L3	23.7	35.41	.87	1.16	6.43	.52	.17	28.74	1.26	.03	98.31	6.97
Phosphate layer A3	14.7	7.2	22.69	.93	.82	.06	.22	50.07	.98	.03	97.78	2.25
Phosphate layer A2	10.8	16.44	22.87	.49	.64	.12	.17	45.42	.81	.02	97.86	3.32
Phosphate layer A1	7.6	20.19	24.48	.48	.87	.14	.17	43.12	.68	.03	97.84	2.94

LOI indicates loss on ignition.

Table 2
Trace element analyses of the phosphate layers (XRF).

Sample (mg/kg)	Cd	As	V	La	Ba	Y	Nd	Se	Sr	Cs	U	La	Ce	W	Pb	Bi
Phosphate layer A3	10	43	314	88	246	159	50	9	961	7	94	149	186	18	17	13
Phosphate layer A2	18	14	587	73	310	144	51	8	824	16	111	153	22	15	15	11
Phosphate layer A1	13	11	433	49	278	84	33	2	725	3	41	150	186	18	14	14

Table 3

Significant element analyses of fluorapatite standards and apatites of the three phosphate layers (electron microprobe analysis).

Sample number	Si	Fe	Mg	Ca	Sr	Na	P	F	Cl	O
<i>Elemental weight percent</i>										
Fluorapatite Standard 1	0.0704	0.0794	0.02	39.21	0.066	0.204	17.69	3.59	0.3684	38.7
Fluorapatite Standard 2	0.0695	0.0787	0.0195	39.24	0.064	0.198	17.69	3.59	0.355	38.7
<i>Elemental weight percent in apatite of the A3 phosphate layer</i>										
11	1.2932	0.1252	0.0912	39.18	0.1965	0.0448	16.18	4.74	0.0008	38.15
12	0.3045	0.0161	0.0554	39.91	0.1497	0.02	16.64	5.06	0.0064	37.84
13	0.716	0.0541	0.0482	39.34	0.1172	0.0222	16.62	5.02	0	38.06
14	2.7143	0.1831	0.132	37.38	0.1021	0.0041	16.16	4.25	0.0275	39.04
15	0.232	0.0408	0.0397	39.83	0.1154	0.0579	16.8	4.93	0.0097	37.94
16	0.598	0.0686	0.0583	40.32	0.142	0.002	16.08	5.12	0	37.62
17	1.1009	0.1171	0.0774	38.83	0.0957	0.0681	16.66	4.63	0.0158	38.4
18	1.2026	0.0936	0.0734	39.66	0.1171	0.0313	16.07	4.7	0	38.06
19	0.9956	0.0987	0.0967	38.94	0.1284	0.0456	16.71	4.58	0.0097	38.39
20	1.3979	0.1306	0.0886	38.74	0.1153	0.0149	16.38	4.79	0.0081	38.33
<i>Elemental weight percent in apatite of the A2 phosphate layer</i>										
1	0.0704	0.0794	0.02	39.21	0.0663	0.2045	17.69	3.59	0.3684	38.7
2	0.0695	0.0787	0.0195	39.24	0.0642	0.1981	17.69	3.59	0.355	38.7
3	0.2062	0.0027	0.0474	39.83	0.0654	0.0757	16.71	5.26	0.0131	37.79
4	0.5149	0.0273	0.0499	39.85	0.1413	0.0603	16.39	5.23	0	37.74
5	2.521	0.2124	0.1275	37.78	0.0776	0.064	15.79	4.89	0.0141	38.52
6	0	0	0.0322	40.17	0.1841	0.0684	16.71	5.16	0.0016	37.69
7	0.2382	0.0269	0.0331	39.76	0.1961	0.0723	16.71	5.15	0.004	37.81
8	0.1817	0.043	0.0362	40.19	0.114	0.1045	16.53	5.09	0.0144	37.69
<i>Elemental weight percent in apatite of the A1 phosphate layer</i>										
9	0.4441	0.1191	0.0581	40.3	0.2009	0.1633	16.03	5.21	0.0107	37.46
10	0.3241	0.1046	0.0651	40.5	0.1927	0.1031	16.13	5.06	0.014	37.51
21	0.0085	0.0451	0.1122	40.51	0.2012	0.1015	16.51	4.86	0.0045	37.65

crystals and some calcareous nodules, and shell and wood (but no vertebrate) fragments. The A2 phosphate layer is medium-grained and moderately sorted, and interbedded with laminated peloid-bearing black shale at top and bottom. It has large wood fragments in its center. The L2 shale contains distinct thin moderately sorted peloidal phosphate laminae and chert nodules, as well as scattered, isolated phosphate peloids at top and bottom. The topmost A3 phosphate layer is carbonate rich, and contains loosely packed medium to fine-grained, moderately sorted peloids. Wood fragments and small pyrite flakes occur at the bottom and the layer coarsens upward from small tightly packed peloids at the base to larger loosely packed peloids at the top.

4.1. Petrology

In thin sections the phosphate rocks are grain-supported, with ovoidal, spherical, and elliptical peloids (ranging from sub-rounded to well rounded) in a blocky calcitic cement (Fig. 6). The peloids are dark brown to yellow depending on their organic content and pyrite inclusions, and range from 30 to 2000 μm in diameter with most around 300–700 μm . The peloids frequently have nuclei and either show rings of secondary phosphate growth (giving an oolitic appearance) or are completely devoid of internal structure. Peloids

have a wide variety of nuclei, such as quartz, ilmenite, and feldspar grains, foraminifera, shell and shell fragments, wood fragments and calcite (Fig. 7A–D). The shell fragments are dominantly of small and thin-shelled molluscs which may be of pelagic species since here are no thick-shelled fragments of benthic organisms. Large fragments of phosphatized wood (up to one centimeter in size) also occur in some thin sections (Fig. 8). Secondary francolite, pyrite, calcite, and silica replace both peloids and cement. Cross-cutting relationships indicate a succession of post-depositional diagenetic changes. Mineral grains, shells, and wood fragments acted as nucleic sites for authigenic apatite precipitation (Fig. 7). Silicification of parts of some apatite peloids (Fig. 9A) was followed by a second phosphate replacement phase of francolite (Fig. 9B). The peloidal grainstones were then cemented by calcite and a further silica precipitation phase filled in micropores and dissolution channels. Pyrite flakes and aggregates are scattered indiscriminately throughout the peloids and matrix and may have been the last mineral to form. Thus, primary authigenic precipitation of apatite was followed by local silica replacement. Secondary phosphatization ensued, followed by a calcite and secondary silica phase, and lastly pyrite deposition. The petrology suggests dominantly anaerobic to disaerobic conditions during deposition and cementation (the abundance of pyrite in peloids and matrix; the scattered

Table 4

Select chemical ratios of the three phosphate layers.

Phosphate layer	CaO/P ₂ O ₅ ratio	F/P ₂ O ₅ ratio	Phosphate layer	CaO/P ₂ O ₅ ratio	F/P ₂ O ₅ ratio	Phosphate layer	CaO/P ₂ O ₅ ratio	F/P ₂ O ₅ ratio
A3	1.46	0.13	A2	1.35	0.09	A1	1.54	0.14
	1.45	0.13		1.35	0.09		1.53	0.14
	1.41	0.14		1.46	0.14		1.50	0.13
	1.45	0.11		1.48	0.14		1.52	0.14
	1.53	0.13		1.46	0.14			
	1.42	0.14		1.47	0.13			
	1.51	0.12		1.45	0.13			
	1.42	0.13		1.48	0.13			
	1.44	0.12						
	1.48	0.13						
	Average ratio	1.45		0.13			1.43	0.12

Table 5

Analyses of selected shale and phosphate samples using NAA, ICP-DES and Leco Furnace instrumentation (Universities of Guelph and Waterloo).

	U (mg/kg)	P (mg/kg)	K (mg/kg)	Th ^r (mg/kg)	Cr (mg/kg)	Zn (mg/kg)	La (mg/kg)	Ce (mg/kg)	Nd (mg/kg)	Ba (mg/kg)	Organic carbon%
<i>Shale samples I/D numbers</i>											
9	19.1	8254	1701	7.5	138	917	23	41	16	140	3.54
12	92.6	59710	3458	6.3	202	626	61	80	39	340	6.69
16	44.5	29894	2964	6.3	192	639	38	57	22	340	3.7
23	18	12114	2072	9.1	97	412	47	90	36	100	2.18
370	70.8	47721	1618	5.9	135	808	48	65	33	290	2.35
59	27.2	15905	1983	7.6	147	981	27	49	19	280	3.63
<i>Phosphate samples I/D numbers</i>											
8, in A3	90.5	105230	1050	4.1	100	164	61	71	31	410	1.85
10 ¹ , in A3	104	101628	719	3.5	112	183	63	71	28	740	1.94
13, in A2	156	106942	667	5.1	100	158	87	101	51	200	1.85
14 ¹ , in A2	182	115629	666	6.1	133	249	111	131	60	370	1.61
17, in A1	159	92488	3126	7.8	311	537	116	160	73	450	3.51
19, in A1	20	13284	525	2.4	38	100	20	38	17	200	.81
27, in A2	161	105256	1018	6	184	413	93	111	58	500	1.26
36 ¹ , in A2	180	109667	660	5.2	114	313	105	129	51	320	2.0

^r Denotes average.

thin shelled pelagic mollusc fragments; and lack of thick-shelled benthic fragments): though the winnowing that concentrated the peloids to give the phosphorites also indicates some bottom water agitation which may have allowed some oxygenated water to mix with anoxic bottom waters at those times.

4.2. Geochemistry

Geochemical analyses of the phosphate and shale layers are in Tables 1–5.

The phosphorus in the Napo Formation is almost exclusively concentrated in the fluoroapatite (see below): no other phosphate minerals were found in any of the samples. In the phosphate layers, there is an excellent linear correlation between U and La (Fig. 10A) and good correlation between U and P, Ce and Nd (Fig. 10B–D). By contrast, in the interbedded black shales, there is an excellent cor-

relation between U and P (Fig. 11A) and only a moderate correlation between U and La (Fig. 11B). The linear correlations between U and organic carbon, and P and organic carbon are poor in both phosphate layers and shales (Tables 1 and 5; Fig. 12); while P and La correlations are moderate (Fig. 13).

Sedimentary phosphate deposits typically have a positive correlation between uranium and phosphate concentrations (Kolodny, 1980; Burton, 1975; Burnett, 1977; Lucas and Abbas, 1989; Follmi, 1996). Here, however, the correlation is stronger for the interbedded shales (R^2 0.99) than for the phosphate layers (R^2 0.68) (Figs. 11A, 10B), though the total concentrations are lower in the shales. This suggests that, although most of the uranium is probably contained either within the apatite lattice or adsorbed onto mineral surfaces, other factors must be affecting the ratios.

Most marine sedimentary phosphate deposits also have high fluorine concentrations (Sheldon, 1969). The Napo phosphates

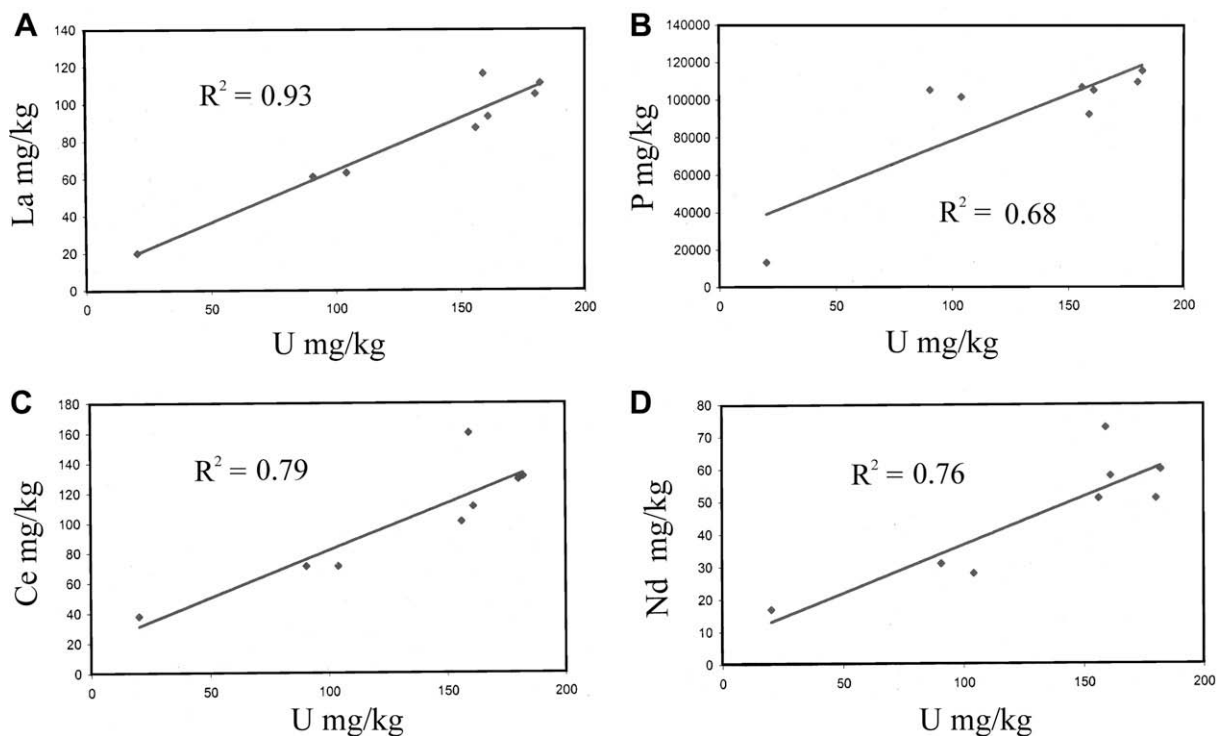


Fig. 10. Linear correlations in phosphate beds between uranium and: (A) lanthanum, (B) phosphorous, (C) cerium, and (D) neodymium.

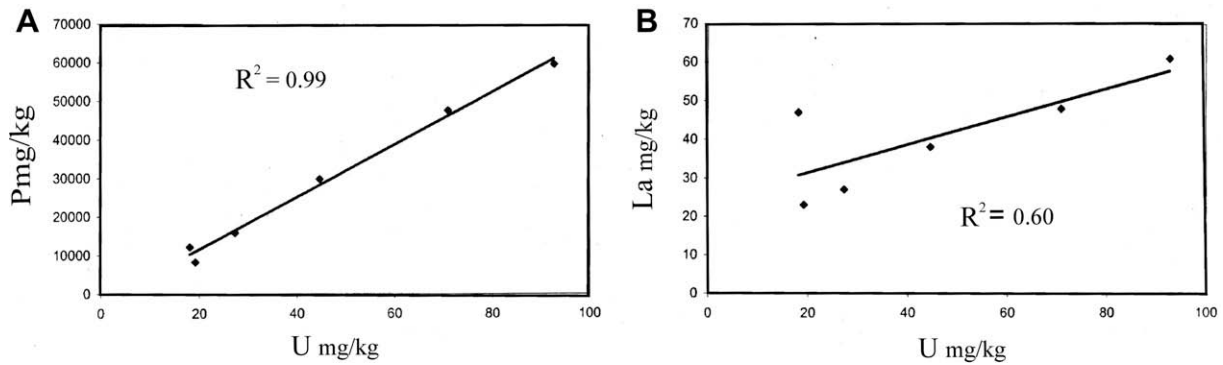


Fig. 11. Linear correlations in shales between uranium and: (A) phosphorous, (B) lanthanum.

have similar elevated fluorine concentrations between 3.59% and 5.26%, compared with 3.59% for the Durango fluoroapatite standard (Table 3). The Napo phosphates are fluorine rich carbonate-fluoroapatites. Microprobe results show that the Napo apatites have an overall F/P_2O_5 ratio of 0.13, thus classifying them as excess fluorine francolites (Szilas, 2002) (Table 4). Veeh et al. (1974) and Soudry et al. (2002), showed that in marine environments with high biological productivity and organic carbon fluctuations, uranium and organic matter concentrations are normally correlated. The Napo phosphates have poor uranium and organic carbon correlations in both the phosphate layers and shale interbeds (Table 5, Fig. 12). The uranium found in the phosphate and shale layers is therefore probably in the apatite and not in the organic matter associated with the phosphates.

Rare Earth Elements (REE) concentrations are normally elevated in phosphorite deposits, (Altschuler, 1980). The measured REE concentrations found in the Napo phosphates are highly enriched compared to the North American Shale Composite (NAS) (Gromet et al., 1984), are typical of marine phosphates, and correlate with uranium (Table 5), while the small Ce depletion anomaly is also typical (Gnadi and Tobschall, 2003). The Napo Phosphorite also has a seawater-like REE distribution found in other sedimentary phosphorites (Jarvis et al., 1994; Shatrov, 2007).

4.3. Depositional environment

In the following sections, the depositional environment of the Napo phosphates will be inferred and compared to upwelling and non-upwelling models for phosphorite genesis.

The Napo phosphates were deposited at the transition from bioclastic limestone deposition to black shale deposition in a back-arc basin along the west coast South America, in an equatorial paleolatitude similar to today and conducive to upwelling currents (Veeh et al., 1973, 1974; Manheim et al., 1975; Burnett, 1977; Baldock, 1985) (see Figs. 1 and 2).

The large coniferous wood fragments and angular detrital grains of quartz, feldspar and ilmenite scattered throughout the three moderately sorted phosphate layers indicates a relatively near-shore depositional environment supplied by first-cycle clastic sediment. Upwellings as first proposed by Kazakov (1937), are believed to play both direct and indirect roles during major phosphogenic episodes, producing vast phosphorite deposits spanning upwards of hundreds of kilometers in length (Sheldon, 1964; Bushinski, 1966; Gulbrandsen, 1969; Gulbrandsen and Robertson, 1973; Manheim et al., 1975; Burnett, 1977; Cook and McElhiny, 1979; Riggs, 1979; Bentor, 1980). In upwelling environments, phosphorites are typically associated with cherts and black shales (Riggs, 1979; Sandstrom, 1990; Glenn et al., 1994).

Evidence from the Napo Formation support the upwelling hypothesis since the phosphate layers in the Upper Napo Formation are interbedded with organic rich black shales, and chert nodules were observed and have been documented elsewhere (Ministerio de Recursos Naturales y Energeticos Direccion General de Geologia y Minas, 1985; Vera, 2001). Phosphate formation and deposition in upwelling environments is largely dominated by authigenic peloidal apatite precipitation, normally accompanied by some post-depositional processes, which concentrate the apatite (Glenn and Arthur, 1988; Follmi, 1996). Observations from the Napo thin sections indicate that the peloidal phosphates were formed authigenically, from phosphate-rich sediments, followed by some post-depositional processes including winnowing and minor compaction. The Napo phosphate peloids are largely centered on mineral grain nuclei and some exhibit an oolitic appearance, indicative of authigenic formation (Lambo, 1993). These observations of paleogeographic location, mineral associations, and mineralogy indicate that the phosphates of the Napo Formation may have been formed in an upwelling environment.

However, studies of modern peloidal phosphorite deposits indicate that phosphogenic episodes may not be solely restricted to environments where prominent upwelling currents occur (O'Brian et al., 1981; Rutenberg and Berner, 1993). Phosphates do not form in many present day upwelling environments but do form in certain non-upwelling environments such as shallow lagoons, estuaries, or deltas, where phosphate can be supplied by fluvial systems containing P and S-rich organic detritus (Riggs, 1979; Glenn and Arthur, 1990; Rutenberg and Berner, 1993). As the terrigenous sediment enters the marine environment, organic detritus begins to settle, primarily with the fine-grained clays. Once phosphate

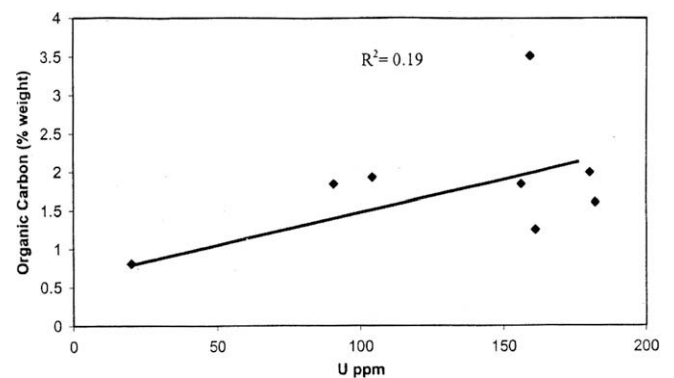


Fig. 12. Poor correlation between organic carbon and uranium in phosphate layers.

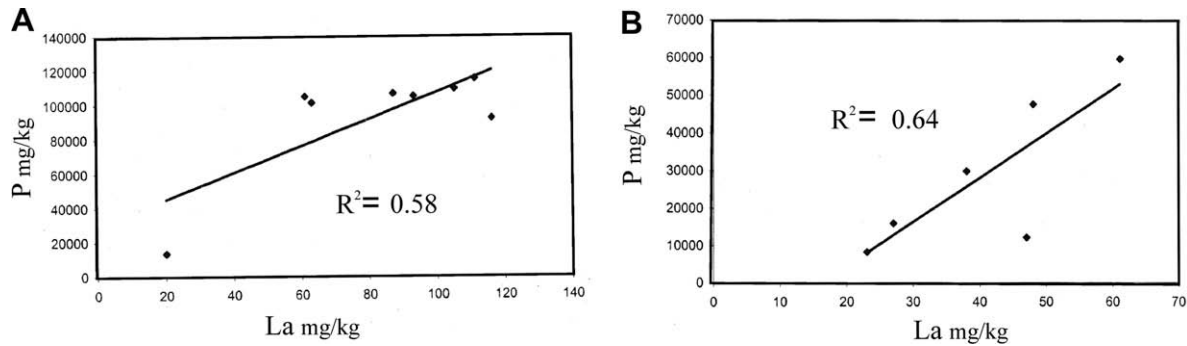


Fig. 13. Linear correlations between phosphorous and lanthanum in phosphate (A) and shale (B) beds.

concentrations reach sufficient concentrations in the sediment, authigenic apatite formation may begin, often coupled with iron oxyhydroxide reduction (Krom and Berner, 1981; Glenn and Arthur, 1988; Lamboy, 1993). Such phosphorite deposits forming in non-upwelling area are normally localized and relatively small compared with the vast phosphorite deposits formed by upwelling currents (Glenn et al., 1994).

Thin sections of the Napo phosphates show abundant land-derived particles, such as large wood fragments and angular unstable mineral grains (feldspar, ilmenite). The Napo phosphorite deposit is only 14 km long, relatively small compared with major global phosphorite deposits (Vera, 2001). Conditions therefore must have been favorable for phosphogenesis in a localized, shallow, quiet marine environment (Shatrov, 2007).

Napo phosphorites have some characteristics of both upwelling and non-upwelling models of phosphorite formation (Table 6). The Napo phosphorites are only 14 km long (though lesser, concentrations extend several hundred kilometers to the south – see Fig. 4): they are too small to be produced by large scale, P-rich upwelling currents, but comparable in scale to a deltaic environment. Such environments, however, are supplied with river-derived clastics, which normally dilute dissolved phosphate concentrations, thus hampering authigenic apatite formation. Glauconite, a common mineral associated with non-upwelling environments, does not occur in the Napo Shale, though it does occur in the glauconitic sandstones of the Middle Napo below (Fig. 3).

Evidence from the Napo Formation supports various aspects of both upwelling and non upwelling hypotheses as in other ancient phosphorites (Hiatt and Budd, 2001). The phosphogenic episode resulting in the formation of the Napo phosphorite occurred at the edge of an open shelf at the junction of bioclastic limestone

and black shale deposition - which is compatible with an upwelling scenario. However, these facies pass laterally into fluvial and deltaic environments certainly less than 100 km to the east (Shanmugam et al., 2000).

A possible interpretation is that upwelling currents carried cold nutrient-rich water onto the shelf edge where it mixed with warm nutrient-rich water supplied by the rivers. The resulting planktonic blooms in the warm water generated vast amounts of marine organic matter. This, together with land derived clays and silts, settled onto the deep shelf where decomposition of the organic matter led to anoxic conditions where dissolved phosphate concentrations increased. Authigenic apatite peloids began to form within the sediment, mainly around available nuclei (over 40% of peloids have a nucleus). Periodic wave and current action then winnowed the sediment and concentrated the phosphatic peloids into moderate to well-sorted grainstone shoals which interfingered with adjacent un-reworked black muds.

These conditions of black shale deposition and peloidal concentration were confined to a relatively short episode in the Upper Napo. The specific conditions conducive to phosphorite formation did not occur at any other time and so a combination of the upwelling and non upwelling hypotheses seem required to explain these phosphorites. The Upper Napo phosphorites, however, also accumulated during the world-wide Coniacian Cretaceous anoxic event recorded in all oceans (Jenkyns, 1980). Photoc zone anoxia seems to be restricted to the early Coniacian, while the transition to the mid-Coniacian probably marks a period of stronger oxygenation (Beckmann et al., 2008). Fluctuations in anoxia and oxygenation at this time may have triggered both the formation of phosphorite pellets and their winnowing to form the phosphorite grainstones.

Table 6

Comparison of characteristics of upwelling and non-upwelling phosphorite-forming environments with characteristics of the Napo Formation.

Criteria	Upwelling environment	Non-upwelling environment
Geographic setting	Spanning hundreds of kilometres along the western deep shelf and slope margins of continents	Localized, confined deposits in shallow quiet marine areas such lagoons, estuaries and deltas
<i>Napo Formation phosphates</i>	<i>Extensive, but patchy, in deep shelf and slope starved sedimentation environments developed during Coniacian oceanic anoxic event (OAE 3)</i>	
Associations	Shale, chert, pelagic organic matter	Shale, sandstone, glauconite, land-derived organic matter
<i>Napo Formation</i>	<i>Within phosphate layers, shale, chert, land-derived phosphates organic matter, glauconite in sandstones</i>	
Biological activity	Large-scale planktonic blooms with limited deep benthic biota	Normal marine shelf biota affected by anoxia
<i>Napo Formation</i>	<i>Relatively abundant pelagic molluscan biota from Phosphates thin section analysis</i>	
Clastic input	Normally low or absent	High
<i>Napo Formation phosphates</i>	<i>Low clastic input during phosphate accumulation</i>	

5. Conclusions

The Napo phosphorites were deposited at the edge of a stable marine shelf during the Upper Cretaceous (Coniacian). During diagenesis of the phosphate rock, uranium was either incorporated directly into the apatite structure, or adsorbed onto mineral surfaces. The proposed model of formation includes aspects from both the traditional upwelling phosphogenic model and key elements from the non-upwelling model. Phosphogenesis was likely triggered, during a change from shallow water bioclastic to deeper water black shale deposition in a delta platform-slope environment, by a number of key factors including strong upwelling currents, high biological activity, plankton blooms, and large amounts of organic matter production and subsequent accumulation. Dissolved phosphate levels increased in the sediment from a combination of anoxic conditions and microbial activity. Once dissolved phosphate levels were high enough, apatite began to form authigenically around nucleic sites including mineral grains, shells, wood fragments, and foraminifera tests forming peloidal fluorine rich carbonate fluorapatite. As the peloids formed, sedimentation continued and dissolved phosphate concentrations diminished. A period of minor winnowing ensued, and as dissolved phosphate concentrations remained low, an intermittent shale layer was deposited separating the various phosphate layers. This process was repeated three times. Diagenetic processes continued as calcite filled the macro pores in the phosphate layers, followed by a quartz phase that created dissolution channels depositing quartz in micro pores and replacing some of the calcitic matrix. The final stage of the process was the formation of pyrite throughout the phosphate layers as a result of decomposing iron and sulphur rich organic matter in strongly anoxic conditions.

The uniqueness of this deposit in the succession of the Oriente Basin may perhaps be attributed to formation during the last of the great oceanic anoxic events (OAE 3) in the Coniacian.

If mined, this phosphate could supply local farmers with a source of inexpensive phosphate fertilizer (Van Straaten, 2002). However, the phosphate rock does contain elevated levels of radionuclides which may make mining hazardous.

Acknowledgements

M. Brookfield acknowledges the generous support of the Institute of Earth Sciences, Academia Sinica, Taipei through its director Bor-ming Jahn. Dylan Hemmings thanks Professor Ramon Vera (Universidad Central de Ecuador) without whose collaboration the project would not have been possible: he also thanks Drs. B. Hart and M. Powell (University of Western Ontario), Dr. S. Landsberger (University of Texas), E. Nevin and G. Byford (Environmental Health and Safety, University of Guelph), Dr. R. Morin (Radiation Institute of Canada) for technical assistance, and G. Wilson, P. Smith, S. Sadura, G. Bassel and T. Degidts for their advice. Earlier manuscripts were greatly improved by the comments of R. Vera, R. Föllmi, Eric Hiatt, and J.M. Ketzer.

References

- Altschuler, Z.S., 1980. The geochemistry of trace elements in marine phosphorites. Part 1. Characteristic abundances and enrichment. Society of Economic Paleontologists and Mineralogists Special Publication 29, 19–30.
- Baldock, I.W., 1985. The Northern Andes: a review of the Ecuadorian Pacific Margin. In: Nairn, A.E.M., Stehli, H., Uyeda, E. (Eds.), *The Ocean Basins and Margins*. Plenum Press, New York, pp. 181–218.
- Beckmann, B., Hofmann, P., März, C., Schouten, S., Sinninghe Damsté, J.S., Wagner, T., 2008. Coniacian–Santonian deep ocean anoxia/euxinia inferred from molecular and inorganic markers: results from the Demerara Rise (ODP Leg 207). *Organic Geochemistry* 39, 1092–1096.
- Bentor, Y.D., 1980. Phosphorites – the unsolved problem. Society of Economic Paleontologists and Mineralogists Special Publication 29, 3–18.
- Burnett, W.E., 1977. Geochemistry and origin of phosphorite deposits of Peru and Chile. *Geological Society of America Bulletin* 88, 813–823.
- Burton, J.D., 1975. Radioactive nuclides in the marine environment. *Chemical Oceanography* 3, 91–191.
- Bushinski, G.I., 1966. The origin of marine phosphorites. *Lithology and Mineral Resources* 3, 292–311.
- Clapperton, C., 1993. *Quaternary Geology and Geomorphology of South America*. Elsevier, Amsterdam, p. 796.
- Cook, P.L., McElhiny, M.W., 1979. A re-evaluation of the spatial and temporal distribution of sedimentary phosphate deposits in the light of plate tectonics. *Economic Geology* 74, 315–330.
- Dashwood, M.F., Abbotts, I.L., 1990. Aspects of the petroleum geology of the Oriente Basin, Ecuador. *Geological Society Special Publication* 50, 89–117.
- Feininger, T., 1975. Origin of petroleum in the Oriente of Ecuador. *American Association of Petroleum Geologists Bulletin* 59, 1166–1175.
- Feininger, T., Bristow, C.R., 1980. Cretaceous and paleocene geologic history of coastal Ecuador. *Geologische Rundschau* 69, 849–874.
- Föllmi, K.B., 1996. The phosphorus cycle, phosphogenesis and marine phosphate rich deposits. *Earth-Science Reviews* 40, 55–124.
- Glenn, C.R., Arthur, M.A., 1988. Petrology and major element geochemistry of Peru margin phosphorites and associated diagenetic minerals: Authigenesis in modern organic-rich sediments. *Marine Geology* 80, 231–267.
- Glenn, C.R., Arthur, M.M., 1990. Anatomy and origin of a Cretaceous phosphorite greensand giant, Egypt. *Sedimentology* 37, 123–154.
- Glenn, C.R., Föllmi, K.B., Riggs, S.R., Baturin, G.N., Grimm, K.A., Trappe, J., Abed, A.M., Galli-Oliver, C., Garrison, R.E., Dyin, A., Jehl, C., Rohrich, V., Sadaquah, R., Schiderlowski, M., Sheldon, R.E., Seigmund, H., 1994. Phosphorus and phosphorites: sedimentology and environments of formation. *Eclogae Geologicae Helveticae* 87, 747–788.
- Gnadi, K., Tobschall, H.J., 2003. Distribution patterns of rare-earth elements and uranium in tertiary sedimentary phosphorites of Hahotoe–Kpogame, Togo. *Journal of African Earth Sciences* 37, 1–10.
- Gromet, L.P., Dymek, R.F., Haskin, L.A., Korotev, R.L., 1984. The North American Shale composite: its composition, major and trace elements characterization. *Geochimica et Cosmochimica Acta* 48, 2469–2482.
- Gulbrandsen, R.A., 1969. Physical and chemical factors in the formation of marine apatite. *Economic Geology* 64, 365–382.
- Gulbrandsen, R.A., Robertson, C.E., 1973. *Inorganic Phosphorus in Seawater*. Environmental Handbook. John Wiley, Chapter 5, pp. 117–140.
- Hiatt, E.E., Budd, D.A., 2001. Sedimentary phosphate formation in warm shallow waters: new insights into the palaeoceanography of the Permian Phosphoria Sea from analysis of phosphate oxygen isotopes. *Sedimentary Geology* 14, 119–133.
- Hunter, V.A., Plint, A.G., Coniglio, M., 2000. A sequence stratigraphic model of a mixed clastic-carbonate shelf system: the Cretaceous Napo Formation, Oriente Basin, Ecuador. In: *GeoCanada 2000 Conference*, May 29–June 2, 2000, Calgary, Alberta, p. 47 (Abstract Volume).
- Jaillard, E., 1996. Sedimentary model for the Oriente Basin of Ecuador during the Cretaceous. *Third ISAG, St Malo, France*, pp. 385–398.
- Jaillard, E., Bengtson, P., Dhondt, A., 2005. Late Cretaceous marine transgressions in Ecuador and northern Peru: a refined stratigraphic framework. *Journal of South American Earth Sciences* 19, 307–323.
- Jarvis, I., Burnett, W.C., Nathan, J., Almbaydin, F.S.M., Attia, A.K.M., Castro, L.N., Flicoteau, R., Hilmy, M.E., Husein, V., Quitwanah, A.A., Serjani, A.A., Zanin, Y., 1994. Phosphorite geochemistry: state of the art and environmental concerns. *Eclogae Geologicae Helveticae* 87, 643–700.
- Jenkyns, H.C., 1980. Cretaceous anoxic events: from continents to oceans. *Journal of the Geological Society of London* 137, 171–188.
- Kazakov, A.V., 1937. The phosphorite facies and the genesis of phosphorites. *Transactions of the Scientific Institute for Fertilizers and Insectofungicides* 142, 93–113.
- Kennerley, J.B., 1980. Outline of the Geology of Ecuador. *Overseas Geology and Mineral Resources*, No. 55.
- Kolodny, Y., 1980. The origin of phosphorite deposits in the light of occurrences of recent seafloor phosphorites (extended abstract). Society of Economic Paleontologists and Mineralogists Special Publication 29, p. 249.
- Krom, M.D., Berner, R.A., 1981. The diagenesis of phosphorus in a nearshore marine sediment. *Geochimica et Cosmochimica Acta* 45, 207–216.
- Kulp, M.A., Miner, M.D., Fitzgerald, D.M., 2007. Subsurface controls on transgressive tidal retreat pathways, Mississippi river delta plain. *USA Journal of Coastal Research Special Issue* 50, 816–820.
- Kummert, P., Casal, C., 1986. Granulometria de Areniscas Cementada con silica, aplicacion a la Determinacion de los Ambientes de sedimentacion en la Formacion Hollin del Campo Bermejo-Sur. IV Congreso Ecuatoriano de Geologia, Minas y Petroleo, Colegio de Ingenieros Geologos de Minas y Petroleos de Pichnicha, Quito, p. 47.
- Lamboy, M., 1993. Phosphatization of calcium carbonate in phosphorites: microstructures and importance. *Sedimentology* 40, 53–62.
- Lebrat, M., Megard, F., Dupuy, C., 1986. Preorogenic volcanic assemblages and the position of the suture between oceanic terrains and the South American continent in Ecuador. *Zentralblatt der Geologische Palaontologische Tesl* 1 (9/10), 1207–1214.
- Lucas, J., Abbas, M., 1989. Uranium in natural phosphorites: the Syrian example. *Science of Geology Bulletin* 42, 223–236.
- Manheim, R., Rowe, G.T., Jipa, D., 1975. Marine phosphorite formation off Peru. *Journal of Sedimentary Petrology* 45, 243–251.

- McClellan, G.H., Lehr, J.R., 1969. Crystal chemical investigation of natural apatites. *American Mineralogist* 54, 1374–1391.
- Ministerio de Recursos Naturales y Energeticos Direccion General de Geologia y Minas, 1985. Proyecto Fosfatos: Investigaciones de Fosfatos Sedimentarios en la Formacion Napo del Oriente. Quito, Ecuador (unpublished report).
- O'Brian, G.W., Harris, J.P., Milnes, A.R., Veeh, H.H., 1981. Bacterial origin of East Australian continental marine phosphorites. *Nature* 294, 442–444.
- Odin, G.S., 1985. Significance of green particles (glaucony, berthierine, chlorite) in arenites. In: Zuffa, G.G. (Ed.), *Provenance of Arenites*. D. Reidel, Dordrecht, pp. 279–307.
- Riggs, S.R., 1979. Phosphorite sedimentation in Florida a model phosphogenic system. *Economic Geology* 74, 285–314.
- Ruttenberg, K.C., Berner, R.A., 1993. Authigenic apatite formation and burial in sediments from non-upwelling continental margin environments. *Geochimica et Cosmochimica Acta* 57, 991–1007.
- Saito, Y., 2001. Deltas in Southeast and East Asia: their evolution and current problems. In: Mumura, N., Yokoki, H. (Eds.), *Global Change and Asia Pacific Coasts*. APN, Kobe, Japan, pp. 185–191.
- Sanders, J.R., 2001. Sedimentology and stratigraphy of a mixed siliciclastic-carbonate shelf system in outcrop: Cretaceous Napo Formation, Oriente Basin, Ecuador. M.Sc. Thesis, London, University of Western Ontario (unpublished).
- Sandstrom, M.W., 1990. Organic matter in Modern marine phosphatic sediments from the Peruvian continental margin. In: Burnett, S.R., Riggs, W.C. (Eds.), *Phosphate Deposits of the World*, vol. 3. Cambridge University Press, Cambridge, pp. 363–375.
- Shanmugam, G., Poffenberger, M., Alava, J.T., 2000. Tide-dominated facies in the Hollin and Nap (T and U) formations (Cretaceous). Sacha Field, Oriente Basin, Ecuador. *American Association of Petroleum Geologists Bulletin* 84, 652–682.
- Shatrov, V.A., 2007. Rare Earth Elements as indicators of formation conditions of Cretaceous phosphorites: evidence from the East European platform. *Doklady Earth Sciences* 4, 567–569.
- Sheldon, R.S., 1964. Paleolatitudinal and paleogeographic distribution of phosphorite. *US Geological Survey Paper* 501C, pp. 106–113.
- Sheldon, R.S., 1969. Geochemistry of Uranium in Phosphorites and Black Shales of the Phosphoria Formation. *US Geological Survey Bulletin* 1054D.
- Soudry, D., Ehrlich, S., Yoffe, O., Nathan, Y., 2002. Uranium oxidation state and related variations in geochemistry of phosphorites from the Negev (southern Israel). *Chemical Geology* 189, 213–230.
- Szilas, C., 2002. The Tanzanian Minjingu Phosphate Rock-Possibilities and Limitations for Direct Application. Ph.D. Thesis, Royal Veterinary and Agricultural University, Copenhagen (unpublished).
- Tschopp, H.J., 1953. Oil explorations in the Oriente of Ecuador. *American Association of Petroleum Geologists Bulletin* 37, 2303–2347.
- Tschopp, H.J., 1956. Upper Amazon Basin geological province. *Geological Society of America Memoir* 65, 296–303.
- Vallejo, C., Hochuli, P.A., Winkler, W., von Salis, K., 2002. Palynological and sequence stratigraphic analysis of the Napo Group in the Pungarayacu 30 well, sub-Andean Zone, Ecuador. *Cretaceous Research* 23, 845–859.
- Van Straaten, P., 2002. Rocks for crops: agrominerals of sub-Saharan Africa. ICRAF, Nairobi, Kenya.
- Veeh, H.H., Burnett, W.C., Soutar, A., 1973. Contemporary phosphorites on the continental margin off Peru. *Science* 181, 844–845.
- Veeh, H.H., Calvert, S.E., Price, N.B., 1974. Accumulation of uranium in sediments and phosphorites on the South-west African shelf. *Marine Chemistry* 2, 189–202.
- Vera, R., 2001. Estudio de prefactibilidad de tratamiento de mineral de fosforita para la produccion de abono. Quito, Ecuador (unpublished report).
- White, H.J., Skopec, R.A., Ramirez, F.A., Rodas, J.A., Bonilla, G., 1995. Reservoir characteristics of the Hollin and Napo formations, western Oriente Basin, Ecuador. *American Association of Petroleum Geologists Memoir* 62, 573–596.
- Wigley, R.A., Compton, J.S., 2006. Late Cenozoic evolution of the outer continental shelf at the head of Cape Canyon, South Africa. *Marine Geology* 226, 1–23.
- Wilkinson, A.F., 1980. Exploration for phosphate in Ecuador. *Transactions of the Institution of Mining and Metallurgy* 550, 553–641.